European Journal of Radiology 114 (2019) 62–68

Contents lists available at ScienceDirect

European Journal of Radiology

journal homepage: www.elsevier.com/locate/ejrad

Ultra-low dose chest computed tomography: Effect of iterative reconstruction levels on image quality

Mercy Afadzi[a,*], Elisabeth Kirkeby Lysvik[a], Hilde Kjernlie Andersen[a], Anne Catrine T. Martinsen[a,b]

[a] Department of Diagnostic Physics, Oslo University Hospital, Oslo, Norway
[b] The Department of Physics, University of Oslo, Oslo, Norway

ARTICLE INFO

Keywords:
Ultra-low dose
ASIR-V
Image quality
Chest CT
Iterative reconstruction

ABSTRACT

Purpose: To optimize image quality and radiation dose of chest CT with respect to various iterative reconstruction levels, detector collimations and body sizes.

Method: A Kyoto Kagaku Lungman with and without extensions was scanned using fixed ultra-low doses of 0.25, 0.49 and 0.74 mGy $CTDI_{vol}$, and collimations of 40 and 80 mm. Images were reconstructed with the lung kernel, filtered back projection (FBP) and different ASIR-V levels (10–100%). Contrast-to-noise ratios (CNR) were calculated for 12 mm simulated lesions of different densities in the lung. Image noise, signal-to-noise ratios (SNR), variations in Hounsfield units (HU), noise power spectrum (NPS) and noise texture deviations (NTD) were evaluated for all reconstructions. NTD was calculated as percentage of pixels outside 3 standard deviations to evaluate IR-specific artefacts.

Results: Compared to the FBP, image noise reduced (5–55%) with ASIR-V levels irrespective of dose or collimation. SNR correlated positively ($r \geq 0.925$, $p \leq 0.001$) with ASIR-V levels at all doses, collimations, and phantom sizes. ASIR-V enhanced the CNR of the lesion with the lowest contrast from 12.7–42.1 (0–100% ASIR-V) at 0.74 mGy with 40 mm collimation. As expected, higher SNR and CNR were measured in the smaller phantom than the bigger phantom. Uniform HU were observed between FBP and ASIR-V levels at all doses, collimations, and phantom sizes. NPS curves left-shifted towards lower frequencies at increasing levels of ASIR-V irrespective of collimation. A positive correlation ($r \geq 0.946$, $p \geq 0.001$) was observed between NTD and ASIR-V levels. NTD of the FBP was not significantly ($p \leq 0.087$) different from NTD of ASIR-V ≤ 20%. The data from the NPS and NTD indicates a blotchier and coarser noise texture at higher levels of ASIR-V, especially at 100% ASIR-V.

Conclusion: In comparison with the FBP technique, ASIR-V enhanced quantitative image quality parameters at all ultra-low doses tested. Moreover, the use of ASIR-V showed consistency with body size and collimation. Hence, ASIR-V may be useful for improving image quality of chest CT at ultra-low doses.

1. Introduction

The use of computed tomography (CT) in diagnostic radiology has increased rapidly due to advances in CT technology and its widespread availability [1]. For instance, chest CT is now the imaging modality of choice for various chest diseases [2–4]. However, the risk of radiation exposure during CT examination has also become a major concern [3,5–8]. Chest CT in particular, has received increasing attention given that the chest is very sensitive to radiation, since some radiosensitive organs (e.g., breast tissue) are located in the chest region [9]. Consequently, various technologies [10] to reduce radiation dose to patient during CT examination have been developed by CT vendors. Nevertheless, dose reduction affects image quality; hence, it is of utmost importance to achieve acceptable image quality with the lowest radiation dose possible. Previous studies have demonstrated the possibility of using low radiation doses for chest CT due to the high lesion-to background contrast [3,11].

Filtered back projection (FBP) has been the standard reconstruction technique in CT imaging for decades. This technique is based on simplified mathematical assumptions of CT imaging; hence it is less

Abbreviations: NPS, noise power spectrum; NTD, noise texture deviation; FBP, filtered back projection; CNR, contrast-to-noise ratios; SNR, signal-to-noise ratios

* Corresponding author.
E-mail address: merafa@ous-hf.no (M. Afadzi).

https://doi.org/10.1016/j.ejrad.2019.02.021
Received 27 August 2018; Received in revised form 3 January 2019; Accepted 16 February 2019

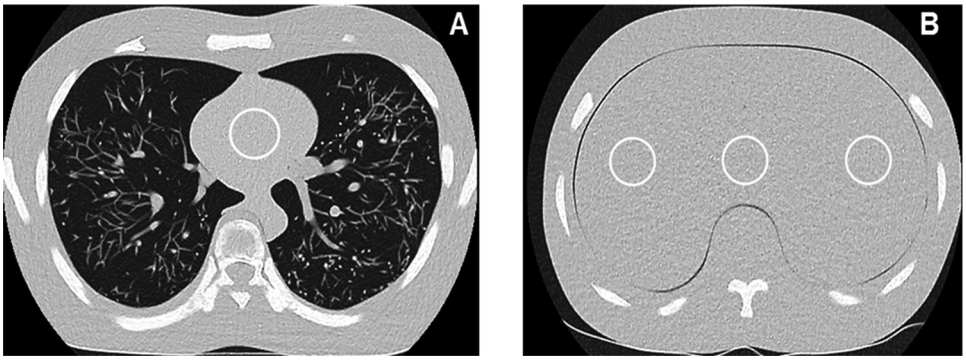

Fig. 1. Measurement of SNR, noise reduction and uniformity in HU in the heart (A) and diaphragm (B).

dependent on data processing power and is a fast reconstruction technique. However, at low radiation doses, images reconstructed with FBP tend to be noisy with streak artifacts and poor low contrast detectability [12,13]. To overcome this limitation, several iterative reconstructions (IR) have been developed taking advantage of the recent advances in computer processing power. IR uses a statistical model of the noise to improve the image on each iteration and the algorithm is vendor specific [14,15]. Compared to the conventional FBP, several studies [3,12,13,16–19] have shown that IR techniques are more effective in acquiring images of high quality at low radiation doses or when high-attenuation metals or body regions are present. Recently, a new generation of adaptive statistical iterative reconstruction (ASIR-V) with potential to achieve significant dose reduction at reconstruction speed comparable to FBP was presented [14].

Image quality in CT can be described by contrast, spatial resolution, image noise and artefacts [9]. Despite the fact that IR algorithm reduces image noise, they have been proven to alter the spatial resolution as well as introduce new artefacts to the image [17,20–23]. IR-specific artefacts (blotchy pixelated appearance) have been reported [22,24,25] to be more pronounced at higher levels of IR. This implies that features for determining optimal image quality might not be captured so well by absolute noise (standard deviation (SD)) and contrast only [9], but information about noise properties, texture, appearance and spatial resolution are also needed. In this study, we aimed to optimize image quality and radiation dose of chest CT for different patient sizes using various ASIR-V levels and two different detector collimations. In particular, the potential of ASIR-V for reducing radiation dose of chest CT, while maintaining image quality has been investigated.

2. Materials and method

2.1. Phantom

In this study, Kyoto Kagaku Lungman phantom (Chest Phantom N1; Kyoto Kagaku Co Ltd, Kyoto, Japan [26]) of 45 cm height with a circumference of 94 cm was used. The phantom has a main body composed of a chest wall, mediastinum (with heart, trachea and pulmonary vessels) and an abdominal (diaphragm) block. The soft tissues and vessels in the phantom were made of polyurethane (1.06 gravity), whereas the synthetic bones were made from epoxy resin and calcium carbonates. Three stimulated spherical lesions made of urethane foam and polyurethane, 12 mm in diameter with Hounsfield units (HU) of -800 (Lesion 1), -630 (Lesion 2) and +100 (Lesion 3) were randomly distributed in the lung for this study. The extensions (anterior and posterior plates) of the chest phantom were added to simulate a bigger size patient.

2.2. Data acquisition and image reconstruction

All data acquisitions were performed on a 16 cm detector GE Revolution CT scanner (GE Healthcare, Milwaukee, WI, USA). The phantom was scanned at fixed ultra-low doses of 0.25, 0.49 and 0.74 mGy volume CT dose index ($CTDI_{vol}$, i.e., 5, 10 and 15 mAs respectively), 120 kVp voltage, 40 and 80 mm collimation, 1.375 pitch, and 0.5 s rotation time. Images were reconstructed with the lung kernel, 2.5 mm slice thickness, filtered back-projection (FBP, ASIR-V 0%) and a new generation of adaptive statistical iterative reconstruction (ASIR-V) with all available levels (10–100%). The same scan protocol was used for the smaller (without extensions) and bigger phantoms (with extensions).

2.3. Image quality analysis

HU and SD were measured with ROIs in the lesions, lung, heart and diaphragm using a picture archiving and communication systems (PACS, software version VB36E, Siemens Healthcare GmbH) workstation. The shape, size and position of the ROIs used for the measurements were kept constant for each dataset by using the copy and paste function in the program. Image noise was estimated by measuring the SD of HU values in a ROI within the heart and the diaphragm (Fig. 1). Reduction in noise in the reconstruction process relative to the FBP was estimated for all dose levels, collimations and reconstructions. Noise reduction in percentage was calculated as the difference in SD between the FBP and the ASIR-V divided by the SD of the FBP multiplied by 100. Signal-to-noise ratios (SNR) were assessed in the heart by dividing the mean HU value by the corresponding SD (Fig. 1).

Contrast-to-noise ratios (CNR) were calculated for the three lesions ensuring no interference of pulmonary vessels with the measurement. CNR of the lesions were calculated as in Eq. (1) [27].

$$CNR = \frac{2(HU_L - HU_A)^2}{SD_L{}^2 + SD_A{}^2} \quad (1)$$

where HU_L and HU_A are the mean HU values measured from ROIs in the lesions and the background (air around the phantom) respectively whereas $SD_L{}^2$ and $SD_A{}^2$ are their corresponding variances (Fig. 2).

Uniformity of HU across the phantom was investigated by calculating the range in HU values between 3 ROIs (one on the left, middle and right) in the diaphragm (Fig. 1B). SNR, CNR and range in HU were estimated for all dose levels, collimations, body sizes and reconstructions.

To fully assess the noise characteristics associated with ASIR-V, the magnitude and texture of the noise was evaluated using NPS. The NPS was estimated as previously described by others [20,28]. Eighteen square ROIs of size 51 × 51 pixels with less than 50% overlap of adjacent ROIs (Fig. 3A) were used for the NPS calculation in this study. It was calculated as the square of the modulus of the 2-D Fourier transform (FT) of the signal as in Eq. (2) [20,21,29].

$$NPS(f_x, f_y) = \frac{P_x P_y}{N_x N_y} |FT(I(x, y))|^2 \quad (2)$$

Fig. 2. Measurement of CNR in Lesion 1(A), Lesion 2(B) and Lesion 3 (C) in the lung.

where f_k is the spatial frequency, P_k is the pixel size and N_k is the number of pixels along the k axis of the ROI. I (x,y) is the signal in a ROI at position (x,y).

To eliminate spikes at low frequencies caused by beam hardening and scattered radiation, a second order polynomial fit was subtracted from the signal I (x, y). This was repeated for 6 images in the diaphragm. NPS(f_x, f_y) was then averaged over the 108 ROIs to reduce noise. NPS(f_x, f_y) was changed to polar coordinates (NPS (r)) by binning the data according to its radial spatial frequency and the average for each bin was taken. To compare the shape of the spectra across the different levels of ASIR-V, each NPS (r) was normalized by its integral across all frequencies (nNPS(r)). Evaluation of IR-specific artefact related to ASIR-V was calculated as described by Fabian and colleagues. That is, NTD was calculated using 6 images from the diaphragm with a square ROI of size 130 × 130 pixels, subdivided into 4 squares (Fig. 3B). Percentage of pixels outside 3 SD from the mean HU value was calculated for each image and then the average NTD was found. NTD and NPS were calculated for all dose levels, collimations, body sizes and reconstructions using a custom-designed MATLAB script.

2.4. Statistical analysis

Statistical analysis was performed with SigmaPlot (version 14; Systat Software Inc, London, UK). To test for significant differences within and across groups, Holm-Sidak Tests (One Way Anova) were used for pairwise comparison and comparison between ASIR-V levels and FBP. Pearson Correlation was used for testing correlation between SNR, peak frequency of NPS, NTD and ASIR-V levels. A p-value below 0.05 was considered statistically significant.

3. Results

3.1. Noise reduction and signal to noise ratio

Fig. 4 shows images from the smaller phantom scanned at 0.25 mGy $CTDI_{vol}$ with 40 mm detector collimation. Images were reconstructed with either the FBP or 80% ASIR-V. In general, image noise reduced with increase in ASIR-V levels and dose irrespective of phantom size. In comparison with FBP (0% ASIR-V), 5–55% relative noise reduction was measured in the heart as the ASIR-V levels increased from 10 to 100 % (Fig. 5). At $CTDI_{vol}$ of 0.74 mGy, 50% ASIR-V reduced image noise by 27% relative to the FBP. At a constant ASIR-V, noise reduction was not dependent on dose or collimation. Consequently, there was a strong correlation ($r \geq 0.925$, $p \leq 0.001$) between the SNR and the ASIR-V level (Fig. 6). Although, SNR was dose dependent, similar SNR were measured for the 40 and 80 mm collimations (Fig. 6). However, higher SNR were measured from the smaller phantom than the bigger phantom at all dose levels and collimation.

3.2. Contrast to noise ratio and uniformity

As expected, the use of ASIR-V increased the CNR in all the lesions in comparison with the FBP (Fig. 7). CNR increased with ASIR-V level at all dose levels and collimation for both phantom sizes. Specifically, CNR of the lesion with the lowest contrast increased from 12.7 to 42.1 as ASIR-V increased from 0–100% for the smaller phantom at 0.7 mGy $CTDI_{vol}$ and 40 mm collimation. Higher CNR were measured in the smaller phantom than the bigger phantom as expected (Fig. 7). HU values measured across the phantom showed no differences in HU between the FBP and ASIR-V levels, as seen in Table 1.

3.3. Noise power Spectrum and noise texture deviation

Data from the NPS calculations show a leftward shift of the peak towards lower frequencies at increasing levels of ASIR-V ($r \geq -0.816$, $p \leq 0.002$) (Fig. 8 and Table 2). The largest shift was observed at 100% ASIR-V at all doses, collimations and body sizes. Slightly higher peak frequencies were measured for higher doses than lower doses. NPS for the bigger phantom had lower peak frequencies than that of the smaller phantom at all dose levels and ASIR-V levels. A strong positive correlation ($r \geq 0.946$, $p \geq 0.001$) was observed between the ASIR-V levels and the NTD. NTD of FBP image was not significantly ($p \geq 0.087$)

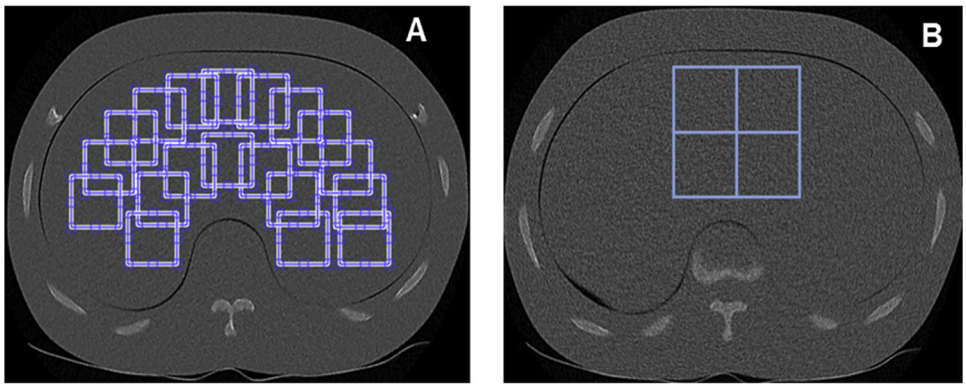

Fig. 3. Measurement of NPS (A) and NTD (B) in the diaphragm.

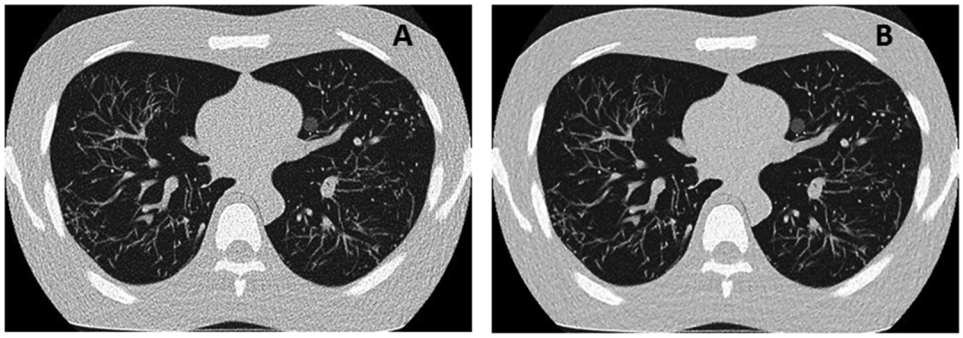

Fig. 4. Images of the smaller phantom scanned at 0.25 $CTDI_{vol}$ and 40 mm collimation. Images were reconstructed with the FBP (A) and 80% ASIR-V (B).

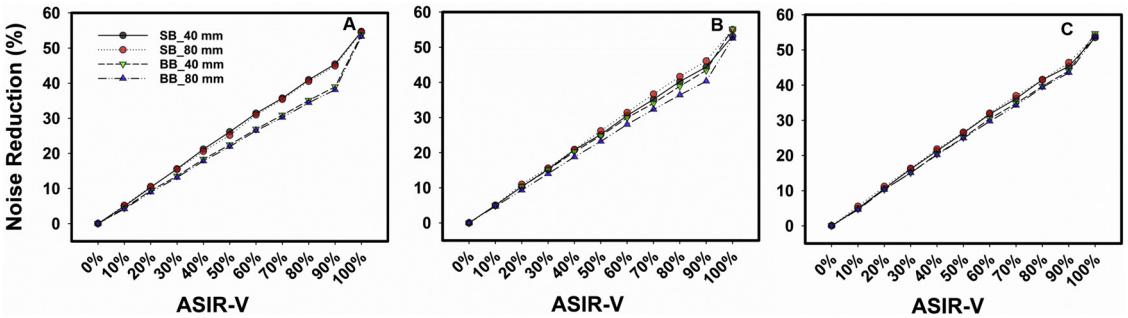

Fig. 5. Percent reduction in noise (SD) between FBP and IR measured in the heart of the small (SB) and big body (BB) size phantoms at different levels of ASIR-V. The phantoms were scanned using fixed ultra-low doses of 0.25 (A), 0.49 (B) and 0.74 mGy (C) $CTDI_{vol}$ and 40 or 80 mm collimation.

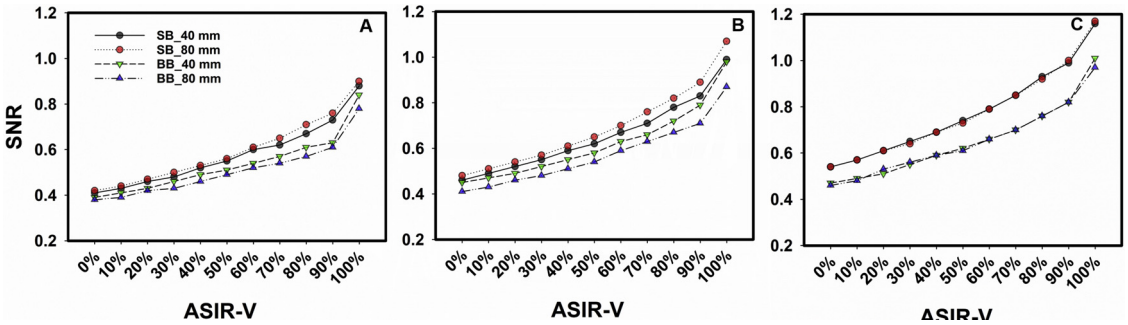

Fig. 6. SNR measured in the heart of the small (SB) and big body (BB) size phantoms at different levels of ASIR-V. The phantoms were scanned using fixed ultra-low doses of 0.25 (A), 0.49 (B) and 0.74 mGy (C) $CTDI_{vol}$ and 40 or 80 mm collimation.

different from ASIR-V ≤ 20% for all the collimations and body sizes, however, it was significantly ($p \leq 0.001$) different compared to NTD of ASIR-V ≥ 20% (Fig. 9). At higher radiation doses (0.49 and 0.74 mGy), NTD for ASIR-V levels of 0 to 80% was not affected ($p \geq 0.089$) by change in body size or collimations (Fig. 9B and C). Conversely, at the lowest radiation dose (0.25 mGy), the NTD of ASIR-V ≥ 40% measured in the smaller phantom with 80 mm collimation was significantly higher ($p \leq 0.026$) than the others (Fig. 9A).

4. Discussion

In this study, we have explored the potential of a new adaptive statistical iterative reconstruction algorithm with respect to image quality and potential for dose reduction. Our results show that the new algorithm reduces image noise and enhances quantitative image quality parameters (SNR and CNR) at ultra-low dose levels (0.25 – 0.74 mGy) compared to conventional FBP in a lung phantom. Literature study [30] has shown that 23–76% dose reduction can be achieved with reduced noise and improved image quality in chest CT when IR methods are used compared to the traditional FBP. Our result is consistent with data from Singh and colleagues [24] who demonstrated that, to obtain acceptable image noise, 70% ASIR is needed to reconstruct chest CT images at radiation dose of 3.5 mGy $CTDI_{vol}$ compared to 9.6 mGy $CTDI_{vol}$ with FBP technique. However, recent studies [31,32] have revealed that model-based IR (MBIR) have the capabilities of enabling further dose reduction over ASIR (statistical IR), while preserving image quality.

Comparing MBIR with ASIR, Kim et al. [32] demonstrated that MBIR technique is better at enhancing image quality, as compared with ASIR at ultra-low dose (0.51 mGy) chest CT. MBIR technique is a purely IR technique which considers both the system geometry and noise statistics of photons and electrons. This IR technique is more complex and advanced than ASIR which is a blend of FBP and IR. Although MBIR gives much better image quality (reduced noise and artefact) at ultra-low doses than ASIR, it has a technical limitation due to the relatively long reconstruction times (30–60 min) which makes it unacceptable in routine clinical use [33]. To overcome this limitation, a new generation of adaptive statistical iterative reconstruction (ASIR-V) has been released. ASIR-V is different from both ASIR and MBIR techniques, due to more advanced noise and object modeling than ASIR but it does not include the system optics in the modelling process as in MBIR [14]. Hence, ASIR-V has the potential to enhance image quality significantly

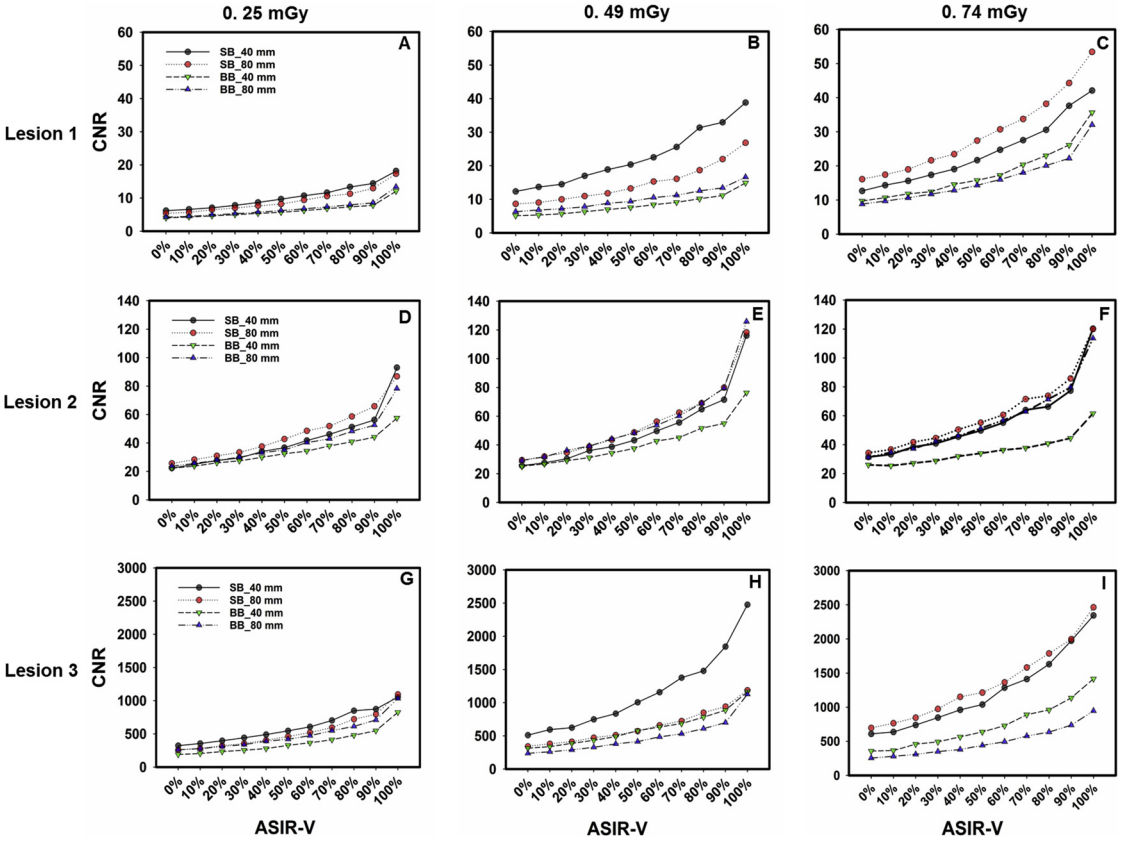

Fig. 7. CNR measured in the three lesions placed in the lung of the small (SB) and big body (BB) size phantoms at different levels of ASIR-V. The phantoms were scanned using fixed ultra-low doses of 0.25 (A, D and G), 0.49 (B, E and H) and 0.74 mGy (C, F and I) $CTDI_{vol}$ and 40 or 80 mm collimation.

at reconstruction speed (25 frames per second) comparable to that of FBP [34]. Moreover, ASIR-V is a hybrid IR technique, thus, it blends IR data with FBP data and so the images are similar to FBP.

At a constant ASIR-V level, percentage noise reduction measured in the present study with the 80 mm collimator was similar to that of the 40 mm. Even though, change in collimator width had minimal effect on the image noise, long scanning times due to narrow detector width has the potential to increase motion artefacts while wide detector collimations may increase x-ray scatter which can decrease image quality [35]. The use of IR methods and anti-scatter grids in front of the detector has been reported to reduce these effects [36]. Variation in HU range measured across the diaphragm in our study was within acceptable range, indicating the absence of cupping artefact even at ultra-low dose.

A shift in peak frequency shows a change in noise texture which can affect the detectability of certain pathology, thus, lowering the diagnostic image quality. According to our results, the NPS peaks shifted towards lower frequencies with increase in ASIR-V level. NPS concentrated at lower frequencies signifies coarse graininess, whereas that at higher frequencies shows finer graininess. A shift toward lower frequencies of ASIR-V NPS has also been reported by Marco et al. [37]. In addition, lower peak frequencies were measured from the bigger phantom than the smaller phantom at all dose levels. Considering the low doses used in this study, these differences might be a result of the higher noise levels in the bigger phantom.

Despite the fact that IR techniques enhance image quality, several studies [2,19,22,24,25] have reported of them introducing new image artefacts (IR-specific artefacts). In the present study, IR-specific

Table 1
Uniformity in HU values (range) measured in a lung phantom at different ASIR-V levels, doses, body sizes and collimations.

ASIR-V	Range in HU measured with 40 mm collimation						Range in HU measured with 80 mm collimation					
	0.25 mGy		0.49 mGy		0.74 mGy		0.25 mGy		0.49 mGy		0.74 mGy	
	Small	Big	Small	Big	Small	Big	Small	Big	Small	Big	Small	Big
0%	4.00	5.00	3.00	4.00	2.00	0.00	0.00	2.00	1.00	4.00	1.00	3.00
10%	4.00	5.00	3.00	4.00	2.00	1.00	0.00	3.00	1.00	4.00	1.00	3.00
20%	3.00	5.00	3.00	4.00	2.00	1.00	0.00	3.00	2.00	4.00	1.00	3.00
30%	3.00	6.00	2.00	4.00	2.00	1.00	0.00	2.00	2.00	4.00	1.00	3.00
40%	3.00	6.00	3.00	4.00	2.00	1.00	0.00	2.00	2.00	4.00	1.00	3.00
50%	3.00	6.00	3.00	4.00	2.00	1.00	0.00	2.00	2.00	4.00	1.00	3.00
60%	3.00	5.00	3.00	4.00	2.00	0.00	0.00	2.00	1.00	4.00	1.00	3.00
70%	3.00	5.00	3.00	4.00	2.00	0.00	1.00	2.00	1.00	4.00	1.00	3.00
80%	3.00	5.00	3.00	4.00	2.00	1.00	0.00	2.00	1.00	4.00	1.00	3.00
90%	3.00	5.00	3.00	4.00	2.00	0.00	1.00	2.00	1.00	4.00	1.00	3.00
100%	3.00	4.00	2.00	4.00	1.00	0.00	1.00	2.00	0.00	4.00	1.00	2.00

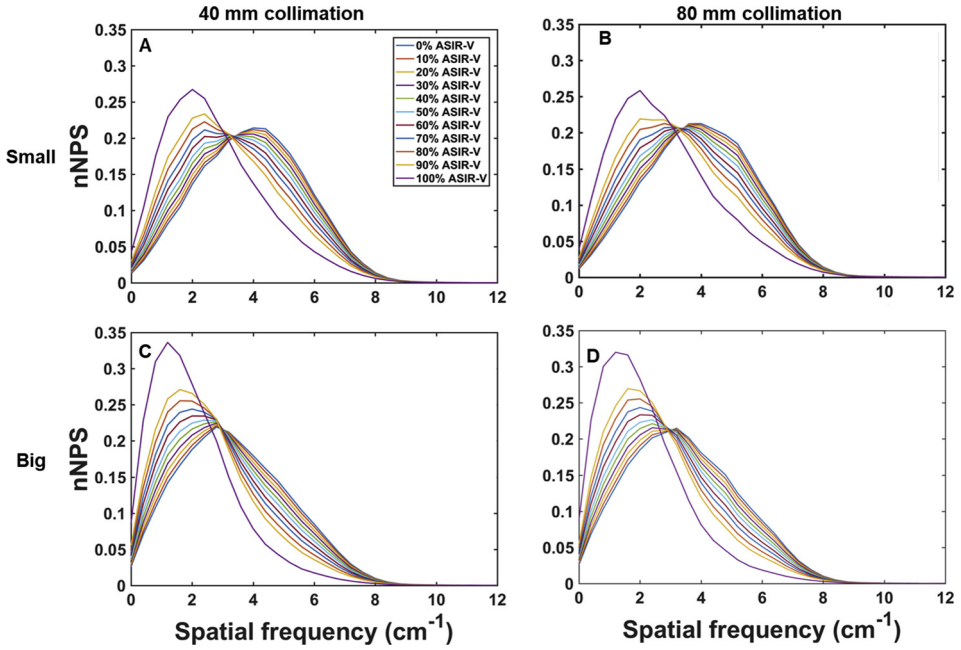

Fig. 8. Normalised NPS (nNPS) measured in the diaphragm of small (A and B) and big (C and D) size phantoms at different levels of ASIR-V. The phantoms were scanned with 0.74 mGy $CTDI_{vol}$ and 40 (A and C) or 80 mm (B and D) collimation.

Table 2
Peak frequency of noise power spectrum (NPS) in a lung phantom at different ASIR-V levels, doses, body sizes and collimations.

ASIR-V	Peak frequency (cm^{-1}) measured with 40 mm collimation						Peak frequency (cm^{-1}) measured with 80 mm collimation					
	0.25 mGy		0.49 mGy		0.74 mGy		0.25 mGy		0.49 mGy		0.74 mGy	
	Small	Big	Small	Big	Small	Big	Small	Big	Small	Big	Small	Big
0%	2.80	1.20	3.20	2.80	4.00	2.80	2.80	1.20	3.20	2.40	4.00	3.20
10%	2.80	1.20	3.20	2.80	4.00	2.80	2.80	1.20	3.20	2.40	3.60	3.20
20%	2.80	1.20	3.20	2.00	4.00	2.80	2.80	1.20	3.20	2.40	3.60	3.20
30%	2.00	1.20	3.20	1.60	4.00	2.80	2.80	1.20	3.20	1.60	3.60	2.40
40%	2.00	1.20	3.20	1.60	3.60	2.80	2.40	0.80	2.80	1.60	3.60	2.40
50%	2.00	0.80	2.80	1.60	3.20	2.40	2.00	0.80	2.80	1.60	3.60	2.40
60%	1.60	0.80	2.80	1.60	3.20	2.00	2.00	0.80	2.80	1.60	3.20	2.00
70%	1.60	0.80	2.80	1.60	2.40	2.00	2.00	0.80	2.80	1.60	3.20	2.00
80%	1.60	0.80	2.00	1.60	2.40	1.60	1.60	0.80	2.40	1.60	2.80	2.00
90%	1.60	0.80	2.00	1.60	2.40	1.60	1.60	0.80	2.40	1.60	2.00	1.60
100%	1.20	0.80	1.60	1.20	2.00	1.20	1.20	0.80	2.00	1.20	2.00	1.20

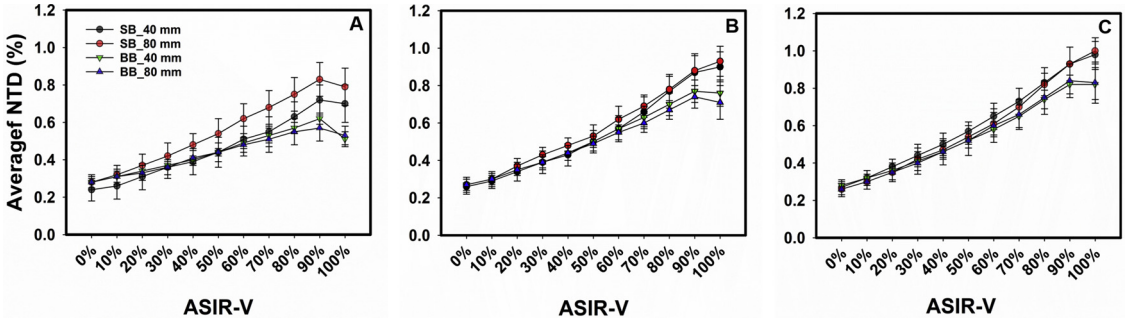

Fig. 9. Average NTD measured in the diaphragm of small (SB) and big body (BB) size phantoms at different levels of ASIR-V. The phantoms were scanned using fixed ultra-low doses of 0.25 (A), 0.49 (B) and 0.74 mGy (C) $CTDI_{vol}$ and 40 or 80 mm collimation.

artefacts were evaluated quantitatively using NTD. Our data revealed no significant differences in the NTD of the FBP images compared to ASIR-V levels ≤ 20%. The results from the NPS and NTD analysis indicate a blotchier and coarser noise texture at higher levels of ASIR-V, especially at 100% ASIR-V. NTD and NPS has been reported to correlate with subjective IR-specific artefacts and noise texture [19–22]. However, Singh and colleagues [24] have reported that 70% ASIR had no effect on the diagnostic confidence, even though IR-specific artefacts were observed at that level. Our results are consistent with the results of a recent study conducted by Tang and colleagues [38] who compared different levels of ASIR-V by evaluating SD and SNR quantitatively as well as image noise, visibility, artefacts and diagnostic acceptability

subjectively. Nevertheless, the lowest dose level used in this study is 22 times and 36 times lower than the average dose used by Tang et al. (5.61 ± 2.48 mGy [38]) and the national dose reference level (9 mGy [39]) respectively.

This study is a quantitative image quality anthropomorphic phantom study enabling systematic and standardized comparisons between dose levels, ASIR-V levels, patient sizes and collimations with respect to several image quality parameters. Hence, anatomical noise, breathing and other patient related effects were not present. Also, inter observer variability and subjective preferences were not assessed in this study. Therefore, a clinical study should be performed to fully validate the conclusions/results of our study.

5. Conclusion

In conclusion, ASIR-V improved image quality for all doses tested for small and large body size. Levels of ASIR-V below 70% may be appropriate for low dose chest CT, based on the results from this study. Also, ASIR-V showed consistency with body size collimation.

Declaration of interest

The authors have no conflict of interest

References

[1] M.L.D. Gunn, J.R. Kohr, State of the art: technologies for computed tomography dose reduction, Emerg. Radiol. 17 (2010) 209–218, https://doi.org/10.1007/s10140-009-0850-6.

[2] S. Singh, M.K. Kalra, R.D. Ali Khawaja, A. Padole, S. Pourjabbar, D. Lira, J.-A.O. Shepard, S.R. Digumarthy, Radiation dose optimization and thoracic computed tomography, Radiol. Clin. North Am. 52 (2014) 1–15, https://doi.org/10.1016/j.rcl.2013.08.004.

[3] S.R. Prasad, C. Wittram, J.-A. Shepard, T. McLoud, J. Rhea, Standard-dose and 50%—reduced-dose chest CT: comparing the effect on image quality, Am. J. Roentgenol. 179 (2002) 461–465, https://doi.org/10.2214/ajr.179.2.1790461.

[4] X. Zhu, J. Yu, Z. Huang, Low-dose chest CT: optimizing radiation protection for patients, AJR Am. J. Roentgenol. 183 (2004) 809–816, https://doi.org/10.2214/ajr.183.3.1830809.

[5] L.F. Rogers, Dose reduction in CT: how low can we go? Am. J. Roentgenol. 179 (2002) 299, https://doi.org/10.2214/ajr.179.2.1790299.

[6] D.J. Brenner, C.D. Elliston, E.J. Hall, W.E. Berdon, Estimated risks of radiation-induced fatal cancer from pediatric CT, Am. J. Roentgenol. 176 (2001) 289–296, https://doi.org/10.2214/ajr.176.2.1760289.

[7] M.K. Kalra, M.M. Maher, T.L. Toth, L.M. Hamberg, M.A. Blake, J.-A. Shepard, S. Saini, Strategies for CT radiation dose optimization, Radiology 230 (2004) 619–628, https://doi.org/10.1148/radiol.2303021726.

[8] D.J. Brenner, E.J. Hall, Computed tomography — an increasing source of radiation exposure, N. Engl. J. Med. 357 (2007) 2277–2284, https://doi.org/10.1056/NEJMra072149.

[9] The 2007 Recommendations of the International Commission on Radiological Protection, ICRP publication 103, 2007, https://doi.org/10.1016/j.icrp.2007.10.003 2007/12/18.

[10] T. Kubo, Y. Ohno, H.U. Kauczor, H. Hatabu, Radiation dose reduction in chest CT—review of available options, Eur. J. Radiol. 83 (2014) 1953–1961, https://doi.org/10.1016/j.ejrad.2014.06.033.

[11] A. Madani, V. De Maertelaer, J. Zanen, P.A. Gevenois, Pulmonary emphysema: radiation dose and section thickness at multidetector CT quantification—comparison with macroscopic and microscopic morphometry, Radiology 243 (2007) 250–257, https://doi.org/10.1148/radiol.2431060194.

[12] Y. Sagara, A.K. Hara, W. Pavlicek, A.C. Silva, R.G. Paden, Q. Wu, Abdominal CT: comparison of low-dose CT with adaptive statistical iterative reconstruction and routine-dose CT with filtered back projection in 53 patients, AJR Am. J. Roentgenol. 195 (2010) 713–719, https://doi.org/10.2214/ajr.09.2989.

[13] R.C. Nelson, S. Feuerlein, D.T. Boll, New iterative reconstruction techniques for cardiovascular computed tomography: how do they work, and what are the advantages and disadvantages? J. Cardiovasc. Comput. Tomogr. 5 (2011) 286–292, https://doi.org/10.1016/j.jcct.2011.07.001.

[14] J. Fan, M. Yue, R. Melnyk, Benefits of ASiR-V Reconstruction for Reducing Patient Radiation Dose and Preserving Diagnostic Quality in CT Exams, White Pap, GE Healthc, 2014 http://www3.gehealthcare.co.uk/~/media/downloads/uk/product/computed-tomography/general/ct-revolutionevoasir-vwhitepaper.pdf (Accessed June 6, 2018).

[15] iDose4 Iterative Reconstruction Technique, Breakthrough in Image Quality and Dose Reduction with the 4th Generation of Reconstruction, Eindhoven Philips Healthc. (2011) (Accessed June 6, 2018), http://incenter.medical.philips.com/doclib/enc/fetch/2000/4504/577242/577249/586938/587315/iDose4_-_Whitepaper_-_Technical_-Low_Res.pdf%3Fnodeid%3D8432599%26vernum%3D-2.

[16] F. Macri, J. Greffier, F.R. Pereira, C. Mandoul, E. Khasanova, G. Gualdi, J.P. Beregi, Ultra-low-dose chest CT with iterative reconstruction does not alter anatomical image quality, Diagn. Interv. Imaging 97 (2016) 1131–1140, https://doi.org/10.1016/j.diii.2016.06.009.

[17] H.K. Andersen, D. Völgyes, A.C.T. Martinsen, Image quality with iterative reconstruction techniques in CT of the lungs—a phantom study, Eur. J. Radiol. Open 5 (2018) 35–40, https://doi.org/10.1016/j.ejro.2018.02.002.

[18] K. Jensen, A.C. Martinsen, A. Tingberg, T.M. Aalokken, E. Fosse, Comparing five different iterative reconstruction algorithms for computed tomography in an ROC study, Eur. Radiol. 24 (2014) 2989–3002, https://doi.org/10.1007/s00330-014-3333-4.

[19] G. Pontone, G. Muscogiuri, D. Andreini, A.I. Guaricci, M. Guglielmo, A. Baggiano, F. Fazzari, S. Mushtaq, E. Conte, A. Annoni, A. Formenti, E. Mancini, M. Verdecchia, A. Campari, C. Martini, M. Gatti, L. Fusini, L. Bonfanti, E. Consiglio, M.G. Rabbat, A.L. Bartorelli, M. Pepi, Impact of a new adaptive statistical iterative reconstruction (ASIR)-V algorithm on image quality in coronary computed tomography angiography, Acad. Radiol. (2018), https://doi.org/10.1016/j.acra.2018.02.009.

[20] J.B. Solomon, O. Christianson, E. Samei, Quantitative comparison of noise texture across CT scanners from different manufacturers, Med. Phys. 39 (2012) 6048–6055, https://doi.org/10.1118/1.4752209.

[21] K.L. Boedeker, V.N. Cooper, M.F. McNitt-Gray, Application of the noise power spectrum in modern diagnostic MDCT: part I. Measurement of noise power spectra and noise equivalent quanta, Phys. Med. Biol. 52 (2007) 4027–4046, https://doi.org/10.1088/0031-9155/52/14/002.

[22] F. Morsbach, L. Desbiolles, R. Raupach, S. Leschka, B. Schmidt, H. Alkadhi, Noise texture deviation: a measure for quantifying artifacts in computed tomography images with iterative reconstructions, Invest. Radiol. 52 (2017) 87–94, https://doi.org/10.1097/rli.0000000000000312.

[23] ICRU Report No. 87: Radiation Dose and Image-quality Assessment in Computed Tomography, 2012/04/01, (2012), https://doi.org/10.1093/jicru/ndt007.

[24] S. Singh, M.K. Kalra, M.D. Gilman, J. Hsieh, H.H. Pien, S.R. Digumarthy, J.-A.O. Shepard, Adaptive statistical iterative reconstruction technique for radiation dose reduction in chest CT: a pilot study, Radiology. 259 (2011) 565–573, https://doi.org/10.1148/radiol.11101450.

[25] S. Singh, M.K. Kalra, J. Hsieh, P.E. Licato, S. Do, H.H. Pien, M.A. Blake, Abdominal CT: comparison of adaptive statistical iterative and filtered back projection reconstruction techniques, Radiology 257 (2010) 373–383, https://doi.org/10.1148/radiol.10092212.

[26] Kyoto Kagaku Co LTD. Chest Phantom N1, Instruction Manual, (2018) (n.d.), http://kyotokagaku.com/products/detail03/pdf/ph-1_manual.pdf.

[27] A. Thitaikumar, T.A. Krouskop, J. Ophir, Signal-to-noise ratio, contrast-to-noise ratio and their trade-offs with resolution in axial-shear strain elastography, Phys. Med. Biol. 52 (2007) 13–28, https://doi.org/10.1088/0031-9155/52/1/002.

[28] S.N. Friedman, G.S.K. Fung, J.H. Siewerdsen, B.M.W. Tsui, A simple approach to measure computed tomography (CT) modulation transfer function (MTF) and noise-power spectrum (NPS) using the American College of Radiology (ACR) accreditation phantom, Med. Phys. 40 (2013) 51907, https://doi.org/10.1118/1.4800795.

[29] S. Dolly, H.C. Chen, M. Anastasio, S. Mutic, H. Li, Practical considerations for noise power spectra estimation for clinical CT scanners, J. Appl. Clin. Med. Phys. 17 (2016) 392–407, https://doi.org/10.1120/jacmp.v17i3.5841.

[30] M.J. Willemink, T. Leiner, P.A. de Jong, Iterative reconstruction techniques for computed tomography. Part 2. Initial results in dose reduction and image quality, Eur. Radiol. 23 (2013) 1632, https://doi.org/10.1007/s00330-012-2764-z.

[31] M. Katsura, I. Matsuda, M. Akahane, K. Yasaka, S. Hanaoka, H. Akai, J. Sato, A. Kunimatsu, K. Ohtomo, Model-based iterative reconstruction technique for ultralow-dose chest CT: comparison of pulmonary nodule detectability with the adaptive statistical iterative reconstruction technique, Invest. Radiol. 48 (2013) 206–212, https://doi.org/10.1097/RLI.0b013e31827efc3a.

[32] H.J. Kim, S.-Y. Yoo, T.Y. Jeon, J.H. Kim, Model-based iterative reconstruction in ultra-low-dose pediatric chest CT: comparison with adaptive statistical iterative reconstruction, Clin. Imaging 40 (2016) 1018–1022, https://doi.org/10.1016/j.clinimag.2016.06.006.

[33] G. Koc, J.L. Courtier, A. Phelps, P.A. Marcovici, J.D. MacKenzie, Computed tomography depiction of small pediatric vessels with model-based iterative reconstruction, Pediatr. Radiol. 44 (2014) 787–794, https://doi.org/10.1007/s00247-014-2899-y.

[34] K. Lim, H. Kwon, J. Cho, J. Oh, S. Yoon, M. Kang, D. Ha, J. Lee, E. Kang, Initial phantom study comparing image quality in computed tomography using adaptive statistical iterative reconstruction and new adaptive statistical iterative reconstruction V, J. Comput. Assist. Tomogr. 39 (2015), https://journals.lww.com/jcat/Fulltext/2015/05000/Initial_Phantom_Study_Comparing_Image_Quality_in.24.aspx.

[35] J.B. Solomon, X. Li, E. Samei, Relating noise to image quality indicators in CT examinations with tube current modulation, Am. J. Roentgenol. 200 (2013) 592–600, https://doi.org/10.2214/AJR.12.8580.

[36] F. Boas, D. Fleischmann, CT artifacts: causes and reduction techniques, Imaging Med. 4 (2012) 229–240, https://doi.org/10.2217/iim.12.13.

[37] P. De Marco, D. Origgi, New adaptive statistical iterative reconstruction ASiR-V: assessment of noise performance in comparison to ASiR, J. Appl. Clin. Med. Phys. 19 (2018) 275–286, https://doi.org/10.1002/acm2.12253.

[38] H. Tang, N. Yu, Y. Jia, Y. Yu, H. Duan, D. Han, G. Ma, C. Ren, T. He, Assessment of noise reduction potential and image quality improvement of a new generation adaptive statistical iterative reconstruction (ASIR-V) in chest CT, Br. J. Radiol. 91 (2017), https://doi.org/10.1259/bjr.20170521 20170521.

[39] A. Widmark, Representative Doses in Norway - 2017: Reporting, Revision and Establishment of New National Reference Values, Norwegian Radiation Protection Authority, Oslo, 2018https://www.nrpa.no/publikasjoner?f=Radiologi.